Opal (Zn/Si) ratios as a nearshore geochemical proxy in coastal Antarctica

Katharine R. Hendry[1] and Rosalind E. M. Rickaby[1]

Received 26 November 2007; revised 15 January 2008; accepted 13 March 2008; published 18 June 2008.

[1] During the last 50 years, the Antarctic Peninsula has experienced rapid warming with associated retreat of 87% of marine and tidewater glacier fronts. Accelerated glacial retreat and iceberg calving may have a significant impact on the freshwater and nutrient supply to the phytoplankton communities of the highly productive coastal regions. However, commonly used biogenic carbonate proxies for nutrient and salinity conditions are not preserved in sediments from coastal Antarctica. Here we describe a method for the measurement of zinc to silicon ratios in diatom opal, $(Zn/Si)_{opal}$, which is a potential archive in Antarctic marine sediments. A core top calibration from the West Antarctic Peninsula shows $(Zn/Si)_{opal}$ is a proxy for mixed layer salinity. We present down-core $(Zn/Si)_{opal}$ paleosalinity records from two rapidly accumulating sites taken from nearshore environments off the West Antarctic Peninsula which show an increase in meltwater input in recent decades. Our records show that the recent melting in this region is unprecedented for over 120 years.

Citation: Hendry, K. R., and R. E. M. Rickaby (2008), Opal (Zn/Si) ratios as a nearshore geochemical proxy in coastal Antarctica, *Paleoceanography*, *23*, PA2218, doi:10.1029/2007PA001576.

1. Introduction

[2] Direct observations of the West Antarctic Peninsula (WAP) have revealed rapid atmospheric and ocean warming together with glacial retreat and ice shelf collapse [*Cook et al.*, 2005; *Meredith and King*, 2005; *Pritchard and Vaughan*, 2007; *Vaughan and Doake*, 1996]. Furthermore, the Antarctic Circumpolar Current pumps modified, nutrient-rich, oxygen-poor warm water from the Upper Circumpolar Deep Water (UCDW) onto the continental shelf along the WAP below 200 m [*Domack et al.*, 1992; *Smith et al.*, 1999]. Warming of the Antarctic Deep Water in recent years [*Clarke et al.*, 2007; *Robertson et al.*, 2002; *Smedsrud*, 2005] and changes in the frequency at which deep water floods the continental shelf may contribute to further glacier ice shelf instabilities through basal melting.

[3] Whether the recent glacial retreat is a result of global warming is controversial because the observational record is limited to the last half century. Geological proxies in rapidly accumulating sediments are required to extend observational records back farther. Sediment and diatom assemblage records from along the length of the WAP show that variability in ice shelf extent, including glacial retreat and basal melting, has occurred over the Holocene [*Bentley et al.*, 2005; *Clapperton and Sugden*, 1982; *Pudsey and Evans*, 2001; *Smith et al.*, 2007a]. However, in this context, it is unclear if the recent observations represent continued retreat after the late Holocene Little Ice Age (LIA), a period of widespread cooling ending in circa 1850. The significance and timing of any LIA in the Southern Ocean is difficult to establish [*Anderson*, 1999], although some evidence indicates more persistent sea ice and cooler temperatures at this time, coincidental with glacier advance near the Muller Ice Shelf [*Domack et al.*, 1995]. The retreat of glaciers through enhanced meltwater flux and increased calving of icebergs may change the freshwater budgets, nutrient levels, and stratification of coastal seas [*Dierssen et al.*, 2002; *Smith et al.*, 2007b]. However, there are few dated geochemical records to supplement the sedimentary and paleontological evidence for glacial retreat. Frequently used paleoproxies for surface temperature, salinity, and nutrient conditions are based on foraminiferal calcite. However, WAP coastal sediments are carbonate free, so we test and apply the trace metal content of diatom opal as a measure of the changing surface water chemistry in a nearshore setting.

2. Background to Approach

[4] Diatom tests or frustrules are formed from hydrated amorphous silica or opal ($SiO_2{\cdot}O{\cdot}3H_2O$, [*Shemesh et al.*, 1988]) into which trace quantities of metals such as aluminum and zinc are incorporated [*Ellwood and Hunter*, 1999; *Van Bennekom*, 1981]. The trace metal content of diatom opal records the availability of trace metals in ambient seawater [*Ellwood and Hunter*, 2000a; *Froelich et al.*, 1992; D. Spoffarth, Oxford University, unpublished data, 2008]. Although aluminum can become secondarily incorporated during diagenesis [*Van Bennekom et al.*, 1989; *van Beueskom et al.*, 1997], the uptake of Zn into opal, expressed as $(Zn/Si)_{opal}$, is thought to faithfully record the ambient concentration of free zinc ions, $[Zn^{2+}]$, in the seawater in which the diatoms grew [*Ellwood and Hunter*, 2000a, 2000b].

[5] The use of trace metal proxies in diatom opal is hampered by the need for separation of frustrules from clays and rigorous cleaning. Diatom tests are of similar size to silt particles and cannot be separated simply by filtration.

[1]Department of Earth Sciences, University of Oxford, Oxford, UK.

0883-8305/08/2007PA001576$12.00

However, biogenic opal is of lower density (<2.16 g cm^{-3}) than lithic minerals (>2.5 g cm^{-3}) and can be separated through the use of differential settling [*Shemesh et al.*, 1988].

[6] Here we demonstrate a heavy liquid flotation technique to separate and clean diatom opal from lithic sediments and a ratio method that allows precise and accurate measurement of $(Zn/Si)_{opal}$ using quadrupole inductively coupled plasma mass spectrometer (Q-ICP-MS). Our core top calibration illustrates the use of $(Zn/Si)_{opal}$ as a proxy for mixed layer salinity and two down-core records from a nearshore setting off the WAP. A ^{210}Pb advection-diffusion model is used to assess sedimentation and bioturbation rates. This mixing model is then used to reconstruct changes in $(Zn/Si)_{opal}$ through time. Our results indicate that recent meltwater flux has lead to a decrease in seawater salinity and enhanced micronutrient availability, which is unprecedented since the end of the LIA.

3. Methods and Materials

3.1. Sampling Procedure

[7] The study site, Marguerite Bay, is located near Adelaide Island and the British Antarctic Survey Rothera Research Station (Figure 1). As part of an Antarctic Funding Initiative project in collaboration with the Rothera Biogeochemical Time Series, we collected a suite of box-cores of rapidly accumulating sediments from Marguerite Bay, near Adelaide Island (WAP) (Figure 1). We employed the technique of allowing the box-corer to settle into the sediments before retrieval to collect the surface layers intact. The presence of a phytodetrital fluff layer on the surface of the box-cores confirmed minimal disturbance. The cores were frozen for transportation back to the United Kingdom. There, opal was separated and cleaned from all the box-core tops, and down core every centimeter for two of the cores (BC388 and BC390), located near the sites of two sediment trap moorings deployed in Marguerite Bay. In addition to box-coring, two moorings were deployed in Marguerite Bay (Figure 1), each of which comprised two sediment traps and a suite of oceanographic instruments. The sediment traps were configured to collect sediment at fortnightly to bimonthly periods throughout 2005–2006. Homogenized splits were obtained from the recovered trap bottles for analysis.

3.2. Separation of Diatom Opal From Sediments

[8] Diatom opal was separated from sediments using a protocol adapted from work by *Morely et al.* [2004]. Briefly, opal is removed from carbonate and organic free sediment by heavy liquid flotation (Sodium polytungstate, LST FastFloat). The opal is rinsed thoroughly and cleaned using a series of reductive and oxidative cleaning steps, rinsed several times in ultrapure water, and then dissolved in 1% Teflon-distilled HF [*Ellwood and Hunter*, 1999; *Shemesh et al.*, 1988].

3.3. Analysis of Opal

[9] Analysis was carried out using an approach adapted from a ratio method for calcite analysis [*Harding et al.*, 2006] on the Perkin Elmer Elan 6100DRC Q-ICP-MS at the University of Oxford (Auxiliary Material[1]). When this ratio method is used for studying metal/Ca ratios in foraminiferal calcite, trace elements and Ca are assessed simultaneously by measuring a minor isotope representing <1% of natural Ca to prevent saturation of the detector [*Harding et al.*, 2006]. However, there is no suitable isotope of Si for this purpose. Instead, a two-step process is used, taking advantage of the relatively high concentrations of Al in diatom opal from coastal sediments: (1) the (Al/Si) ratio is measured in a diluted aliquot of sample (10–20 ppm Si), and (2) the metal/Al ratio is measured in a separate aliquot of the same sample (100–200 ppm Si). The metal/Si ratio is then calculated by multiplication,

$$\left(\frac{X}{\mathrm{Si}}\right)^{\mathrm{Sample}}_{\mathrm{mol}} = \left\{\left(\frac{X}{\mathrm{Al}}\right)^{\mathrm{Sample}}_{\mathrm{Intensity}} \times \left(\frac{\mathrm{Al}}{X}\right)^{\mathrm{Std}}_{\mathrm{Intensity}}\right\} \times \left\{\left(\frac{\mathrm{Si}}{\mathrm{Al}}\right)^{\mathrm{Sample}}_{\mathrm{Intensity}} \times \left(\frac{\mathrm{Al}}{\mathrm{Si}}\right)^{\mathrm{Std}}_{\mathrm{Intensity}}\right\} \times \left(\frac{X}{\mathrm{Si}}\right)^{\mathrm{Std}}_{\mathrm{mol}}. \quad (1)$$

[10] It is important to note the incorporation of Al in sedimentary diatom opal is highly variable and significantly affected by diagenesis [*Dixit et al.*, 2001; *van Beueskom et al.*, 1997], which limits the use of $(Al/Si)_{opal}$ as a paleoceanographic proxy. However, here we are not aiming to interpret the $(Al/Si)_{opal}$ data but to use them to obtain $(Zn/Si)_{opal}$ through simultaneous measurements.

3.4. Testing the Method

[11] We can demonstrate our approach yields robust measurements of (Zn/Si) from cleaned diatom opal. Four requirements must be met for this method to successfully measure Zn in diatom opal. First, the cleaning procedure must separate opal from clay particles. Scanning electron microscope (SEM) images show the particles to be clean; in particular, the intricate frustrule pores are clear of particulates (Figure 2). In addition, sequential leaching experiments were carried out on core top material. Dilute HF was added to the cleaned sample in an acid-cleaned centrifuge tube, sonicated, and left at room temperature. After 30 min, the tube was centrifuged for 1 min and the supernatant was removed, fresh HF was added, and the procedure was repeated. Aliquots of the supernatant were kept and immediately diluted with 1% HNO_3 for analysis as in section 3.3. The dissolution experiments show that (1) Al decreases to a plateau after ~20% dissolution, suggesting the persistence of a surface aluminosilicate "contaminant phase," which can be removed by a prewash of HF (Auxiliary Material), and (2) Zn is not impacted by dissolution (Figure 3). The intensities of some possible contaminant metals were also measured. Ca, Fe, Mg, and U intensities fell with degree of dissolution. Ba and Mn showed no consistent behavior as the sample dissolved but were generally low (~1 and ~1–10 μmol mol^{-1} Si, respectively) (Auxiliary Material) and in

[1]Auxiliary materials are available in the HTML. doi:10.1029/2007PA001576.

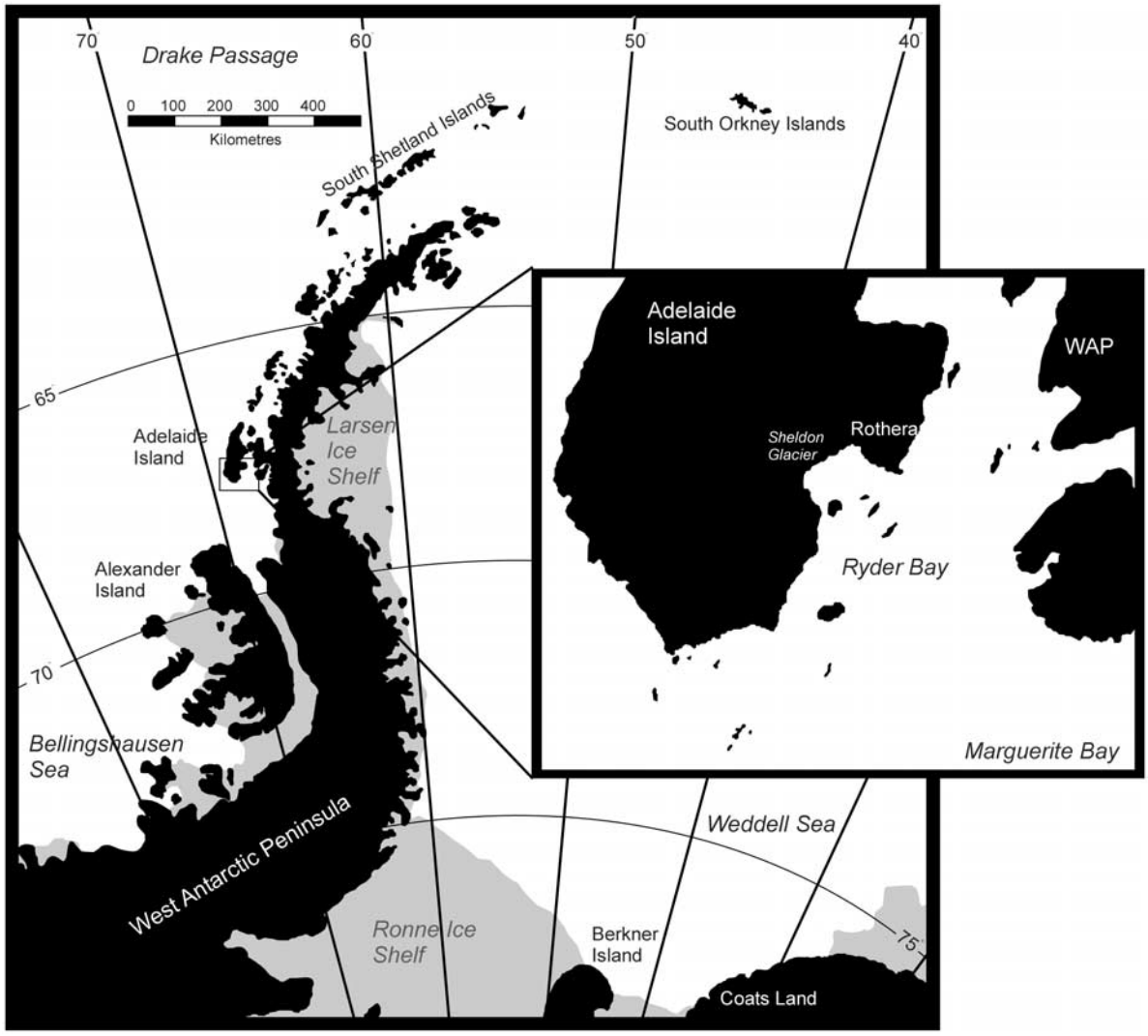

Figure 1. Map of West Antarctic Peninsula showing the location of Rothera Point, the Sheldon Glacier, Marguerite Bay, and Ryder Bay off the southern coast of Adelaide Island. Also shown are core (gray circles) and sediment trap sites (stars) within Marguerite Bay.

agreement with published values [*Dehairs et al.*, 1980; *Gonneea and Paytan*, 2006; *Ho et al.*, 2003; *Martin and Knauer*, 1973]. Cd was rarely above the limit of detection. Hence average $(Zn/Si)_{opal}$ ratios are measured routinely from samples that have undergone 20% dissolution to remove the initial contaminant phase. The nature of this contaminant phase in the opal samples is not clear. Studies of opal surface chemistry suggest Al is only adsorbed at neutral to high pH [*Dixit and Van Cappellen*, 2002], and recent investigation of opal surfaces using energy dispersive X-ray spectrometer spot analysis suggests against surface coatings [*Lal et al.*, 2006]. Unlike Fe and Mn, Zn intensities do not correlate with Al, suggesting the metals do not share a similar source (e.g., Figure 7). This confirms we are measuring the Zn content of the opal, rather than any clay contaminant or other adsorbed material.

[12] Second, the opal must be dissolved cleanly without any loss of Si. Opal can be dissolved in three reagents: $NaCO_3$, NaOH, and HF. The addition of both $NaCO_3$ and NaOH leads to a (1) a high-Zn blank and (2) high-Na matrix which may result in analytical imprecision using Q-ICP-MS. The Na matrix would require removal through ion exchange, increasing the risk of Zn contamination. Hence it was decided to dissolve the samples in HF. Two reactions are possible during the addition of HF to silica, resulting in either the formation of silicon tetrafluoride or hexafluoride (SiF_4 and SiF_6, respectively). The formation of volatile SiF_4 may lead to loss of Si from solution and is undesirable for this method. The formation of the more soluble SiF_6 is favored by using dilute solutions of HF in excess and reacting at low temperatures [*de la Rocha et al.*, 1996]. Theoretically, when dissolving hydrated amorphous silica in HF, the silicofluoride ions remain in solution, provided the system remains below boiling temperature [*Dolezal et al.*, 1968]. For each sample, no more than 2 mg of silica was used and reacted with 0.25 N HF (1% Teflon-distilled HF diluted with Milli-Q water) in excess at room temperature.

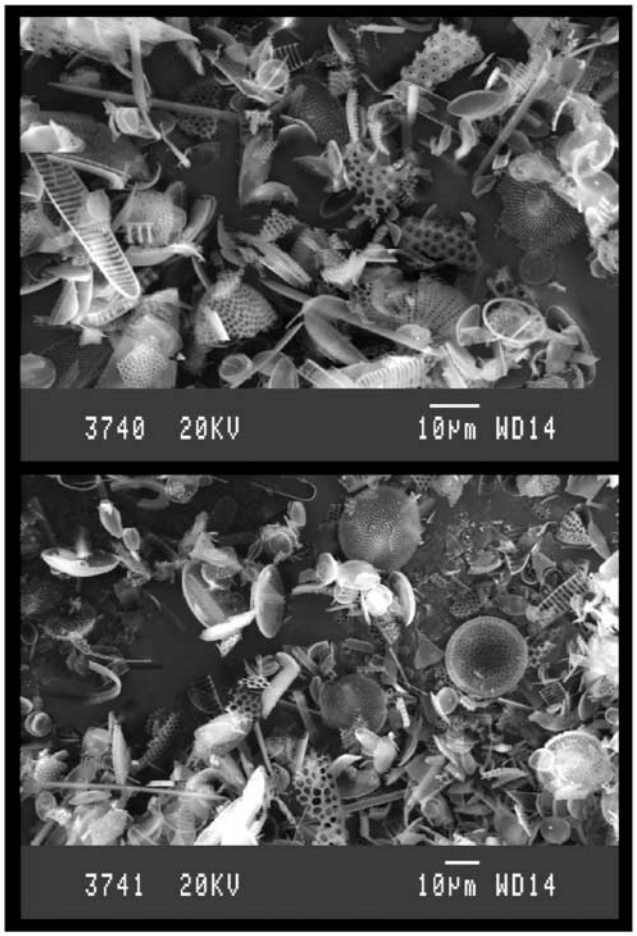

Figure 2. Scanning electron microscope images of separated and cleaned diatom opal from box-core material. The opal is separated from the sediments using a heavy liquid flotation, rinsed thoroughly, then cleaned using a series of reductive and oxidative cleaning steps. Scale bar shows 10 μm.

Tests indicate that, within error, this method yields 100% Si (Auxiliary Material).

[13] Third, the external reproducibility of the method was assessed by measuring both in-house and reference standards. Within-analysis reproducibility was found to be ~0.6%, and long-term reproducibility, measured over the period of 12 months, was found to be ~2% (Auxiliary Material).

[14] Fourth, we can show a good level of reproducibility between samples from the same locality and depth which have undergone the full cleaning and dissolution procedure entirely separately. Repeat measurements of core top material agree well with dissolution experiments (Figure 3).

[15] Our sediment trap and box-core $(Al/Si)_{opal}$ and $(Zn/Si)_{opal}$ values range within published values determined from a variety of methods, providing an additional line of evidence suggesting that the processed opal is sufficiently clean. In particular, the aluminum results, which might be expected to be most affected by clay contamination, correspond well with values from microprobe analysis of core top material [*van Beueskom et al.*, 1997]. $(Zn/Si)_{opal}$ values are similar to down-core records from the Southern Ocean [*Ellwood and Hunter*, 2000b; K. R. Hendry and R. E. M. Rickaby, unpublished data, 2008] and are lower than recent published values for down-core opal [*Lal et al.*, 2006]. From all of the above, we have demonstrated our ability to measure the true Zn content of sedimentary opal, and our measurements are robust and repeatable.

3.5. The ^{210}Pb Dating

[16] The productive summer months and proximity to glaciers yield rapid accumulation of sediments. These high-sedimentation rate cores are ideally situated to preserve a record of recent glacial retreat and its impact on the micronutrient chemistry of the coastal surface waters over centennial timescales. However, these cores were taken from relatively shallow waters (Table 1) and may experience significant mixing by bioturbation. Lead 210 dating can be used, along with a simple advection-diffusion model, to assess sedimentation and mixing rates.

[17] Lead 210 dating of core material from BC388 and BC390 was carried out at the University of Sussex, United Kingdom (Auxiliary Material). The near constant ^{210}Pb activity at depth approximates the supported ^{210}Pb which is measured using the ^{226}Ra daughter product, ^{214}Pb. The excess ^{210}Pb, $^{210}Pb_{xs}$, was calculated by subtracting the supported ^{210}Pb given by the ^{214}Pb activities (Figure 4).

[18] The decay of ^{210}Pb (half-life of 22 years) can be used to calculate sedimentation rates. However, bioturbation can significantly smooth geochemical signals within the mixed layer of sediments and is prevalent in shallow, nearshore marine environments [*Kim and Burnett*, 1988]. Lead 210 for more than 100 years in the sediments and exhibits an exponential profile which approximates the depth of the mixed layer [*Buffoni et al.*, 1992; *Henderson et al.*, 1999; *Nozaki et al.*, 1977; *Peng et al.*, 1979].

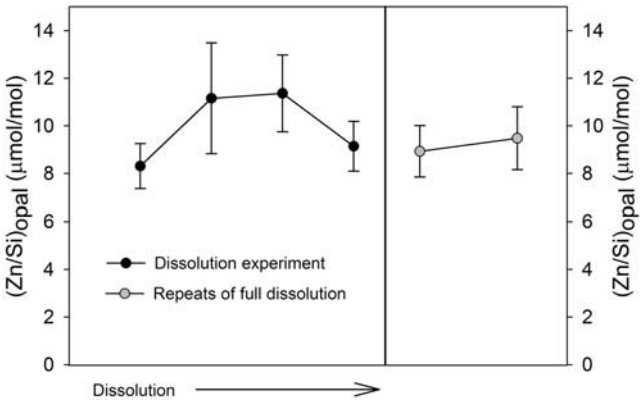

Figure 3. $(Zn/Si)_{opal}$ of box-core top sample (BC388) throughout sequential dissolution. Also shown are $(Zn/Si)_{opal}$ results for repeats, for which different samples were taken through the whole separation and cleaning procedure, showing a high reproducibility in the method. Error bars are $\pm 2\sigma$.

Table 1. Core Top and Sediment Trap Opal Chemistry[a]

Code	Latitude, deg	Longitude, deg	Depth, m	Al/Si, g g^{-1}	Zn/Si, μmol mol^{-1}
BC383	−66.72	−70.45	578	0.0016 (0.0001)	1.17 (0.17)
					1.43 (0.16)
BC384	−67.68	−71.20	504	0.0066 (0.0005)	3.11 (0.32)
BC385	−68.02	−70.52	845	0.0079 (0.0006)	2.75 (0.28)
BC386	−68.03	−70.44	863	0.0151 (0.0008)	3.70 (0.31)
BC388	−67.57	−68.23	505	0.0263 (0.0013)	8.92 (0.54)
BC390	−67.93	−68.40	810	0.0075 (0.0005)	5.59 (0.34)
BC391	−67.86	−68.19	814	0.0053 (0.0003)	4.70 (0.35)
Sediment trap (n = 4)[b]	−67.57	−68.23	125	0.00024	11.1
Sediment trap (n = 13)[b]	−67.93	−68.40	200	0.00012	10.7

[a]Sediment trap values are mean values for n trap bottles, weighted for contribution to annual mass flux. Numbers given in parentheses are errors for the core top (1σ).
[b]From K. R. Hendry and R. E. M. Rickaby (unpublished data, 2008).

[19] The sedimentation and bioturbation processes can be modeled by diffusion and advection, respectively. The model assumes that there is no nonlocal mixing (i.e., discontinuous mixing processes), which is reasonable given the simple activity-depth profile. In addition, it is assumed the $^{210}Pb_{xs}$ profile does not change with time and that sediment porosity is constant with depth [*Henderson et al.*, 1999].

[20] The $^{210}Pb_{xs}$ activity follows the equation [*Anderson et al.*, 1988]

$$D\frac{\partial^2 A}{\partial z^2} - w\frac{\partial A}{\partial z} - \lambda A = 0, \quad (2)$$

where D is the mixing rate (cm^2 a^{-1}), A is the $^{210}Pb_{xs}$ activity, z is the depth (cm), w is the sedimentation rate (cm a^{-1}), and λ is the decay constant for lead 210 (0.0311 a^{-1}). The solution to this equation is

$$A = A_0 e\left(\frac{w - \sqrt{(w^2 + 4D\lambda)}}{2D}z\right), \quad (3)$$

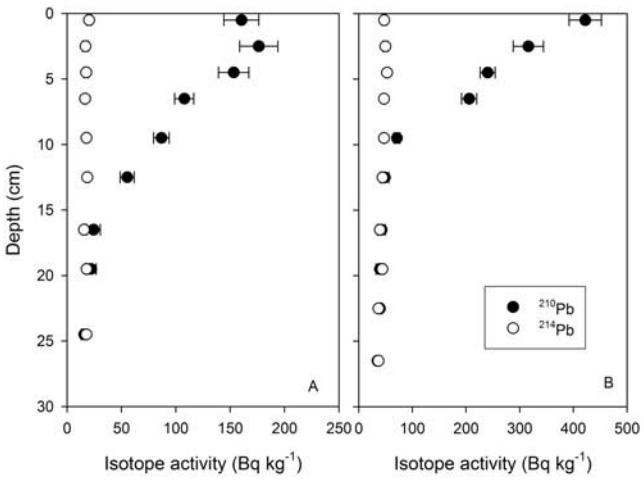

Figure 4. Box-core ^{210}Pb and ^{214}Pb profiles for (a) BC388 and (b) BC390 (error bars are ±2σ). Measurements were carried out at the University of Sussex (A. Cundy, unpublished data, 2006).

where A_0 is the $^{210}Pb_{xs}$ activity at the sediment-water interface. Exponential curves were fitted by least squares to BC388 and BC390 to obtain values for w and D in Marguerite Bay. Errors were estimated by substituting extreme values for surface activity, A_0. For BC388, w = 0.14 cm a^{-1} (±0.10), and for BC390, w = 0.13 cm a^{-1} (±0.08). The maximum ages for the core bases calculated using these sedimentation rates are 214 (±90) years for BC388 and BC208 (±80 years) for BC390.

3.6. Other Analyses

[21] Simple grain size analysis was carried out on BC388: Two weighed samples were taken from each depth, sieved at 63 μm, and reweighed to calculate the percentage coarse fraction. Clay mineralogy was analyzed using energy dispersive X-ray (EDX) and X-ray diffraction (XRD) (Department of Materials Science, Begbroke, Oxford) on dried, powdered samples from box-core BC388. Species counts were carried out on opal, which had been separated using the heavy liquid method, by point counting following published protocol [*Burckle and Cirilli*, 1987; *Burckle et al.*, 1982]. These counts may suffer from bias if some of the smaller or denser species (e.g., *Chaetoceros* resting spores) are lost during the separation procedure and hence should not be considered as true population analyses.

4. Results and Discussion

4.1. Core Top and Sediment Trap Calibration

[22] Box-core top opal show values of $(Al/Si)_{opal}$ from 0.002 to 0.027 g g^{-1} and $(Zn/Si)_{opal}$ from 1.2 to 9.2 μmol mol^{-1} (Figure 5 and Table 1). Sediment trap $(Al/Si)_{opal}$ and $(Zn/Si)_{opal}$ results range from 0.00002 to 0.0003 g g^{-1} and 3.6 to 27 μmol mol^{-1}, respectively (Table 1). Both the sediment trap and core top values compare well with published values [*Collier and Edmond*, 1984; *Ellwood and Hunter*, 2000b; *van Beueskom et al.*, 1997].

[23] In the Marguerite Bay region, the sediment trap and core top $(Zn/Si)_{opal}$ analyses show a strong correlation with mixed layer salinity (Figure 5). This relationship is also consistent with additional data from other Southern Ocean core tops [*Ellwood and Hunter*, 2000b; K. R. Hendry and R. E. M. Rickaby, unpublished data, 2008].

[24] The impact between freshwater and the availability of organic ligands which dominate Zn complexation in

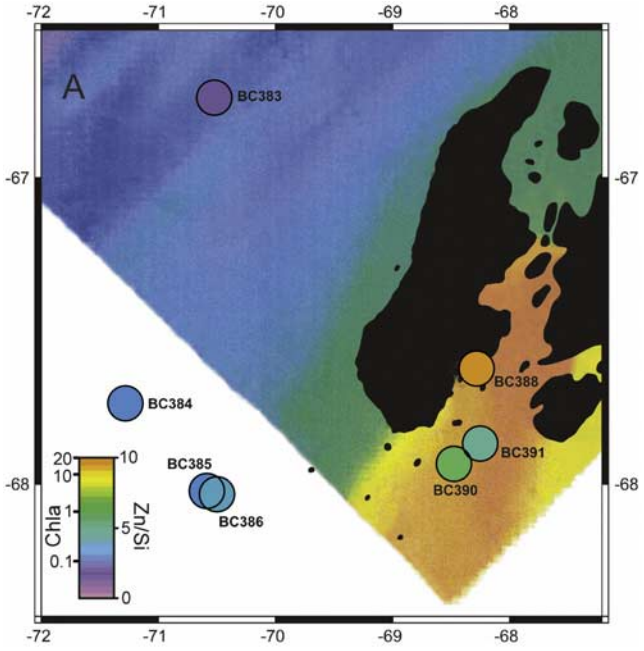

Figure 5a. Map showing box-core top locations, $(Zn/Si)_{opal}$ (filled circles) and chlorophyll *a* distribution in the photic zone, January 1997 (background color contours).

seawater provides the most likely explanation for the relationship between $(Zn/Si)_{opal}$ and salinity. However, there are two alternative hypotheses for the mechanism behind our salinity proxy. First, freshwater sources could dominate Zn input into the Southern Ocean. Field studies based in the Alps show that subglacial water can be a significant source of Zn to stream waters [*Mitchell et al.*, 2001]. There are limited data for Antarctica, but one study in the Ross Sea showed elevated Zn content of glacial meltwater [*Sheppard et al.*, 1997]. A simple mass balance model can be used to assess the impact of freshwater inputs on total Zn concentrations (equation (4)),

$$f_{FRESH} \times S_{FRESH} + (1 - f_{FRESH}) \times S_{CDW} = S_{TOTAL}, \quad (4)$$

where f_{FRESH} is the fraction of meltwater, S_{FRESH} is the salinity of freshwater (taken as 0.5), and S_{CDW} is the salinity of UCDW (taken as 34.6) [*Meredith et al.*, 2008]. Equation (4) was solved for the fraction of freshwater input, f_{FRESH}, and the resulting Zn concentration was calculated assuming [Zn] of UCDW waters to be 5 nM [*Löscher*, 1999], and [Zn] of meltwaters was calculated to range from [Zn] in snow (0.15 nM) [*Boutron et al.*, 1990] to 5.4 nM [*Sheppard et al.*, 1997]. Even the highest estimate of meltwater Zn content results in an onshore-offshore [Zn] decrease of less than 1%. In contrast, our $(Zn/Si)_{opal}$ results are consistent with 1 order of magnitude increase in $[Zn^{2+}]$, which suggests total input of dissolved Zn from meltwaters is unlikely to be significant.

[25] Second, freshwater input enhances growth rates, which could also increase the rate of Zn uptake into opal. In Marguerite Bay, there is a close coupling of salinity and biological productivity (Figure 5). Phytoplankton production is controlled, at least in part, by freshwater input from glacier melting and calving because of the supply of nutrients to the surface waters and the contribution to the vertical stability of the water column [*Dierssen et al.*, 2002]. Zn is an essential element for diatom photosynthesis [*Morel and Price*, 2003], so higher growth rates could result in an increase in cellular uptake of Zn^{2+} and incorporation of Zn into opal [*Ellwood and Hunter*, 2000a]. Furthermore, inputs of micronutrients, in particular iron, from coastal sources could decrease silicic acid pumping, resulting in thinner frustrules and higher N:Si and C:Si uptake ratios [*Brzezinski et al.*, 2002; *Crosta and Shemesh*, 2002; *Crosta et al.*, 2002]. Increased productivity resulting from micronutrient input could increase $(Zn/Si)_{opal}$ ratios if Zn pumping is increased with C and N uptake. Indeed, our preliminary findings from sediment trap opal show a clear seasonal trend in $(Zn/Si)_{opal}$, increasing during the summer months when both growth rates and meltwater input are greatest. However, when all the available core top and sediment trap data are compiled, there is a more significant correlation between mixed layer salinity than chlorophyll *a*, suggesting the impact of meltwater on seawater complexation is the more dominant control on opal chemistry (K. R. Hendry and R. E. M. Rickaby, unpublished data, 2008). Regardless, the upturn in $(Zn/Si)_{opal}$ signifies enhanced melting because productivity is tied so closely to meltwater production in this region through the release of nutrients and water column stratification.

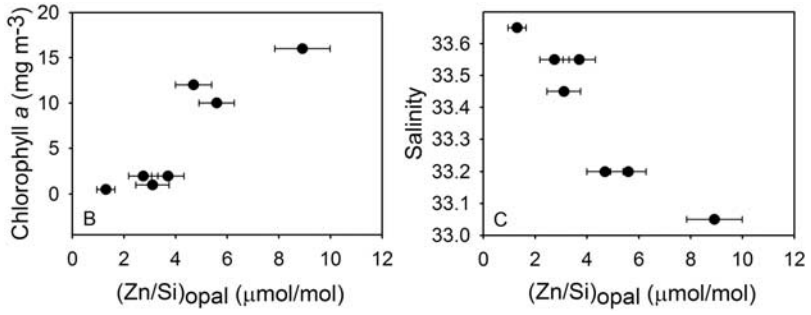

Figure 5b. Correlation between chlorophyll *a* and mixed layer salinity from January 1997 [*Smith et al.*, 1999] and $(Zn/Si)_{opal}$ for core tops. Mixed layer salinity (*S*) is related to $(Zn/Si)_{opal}$ by the equation $S = -0.0828\ (Zn/Si_{opal}) + 33.744$.

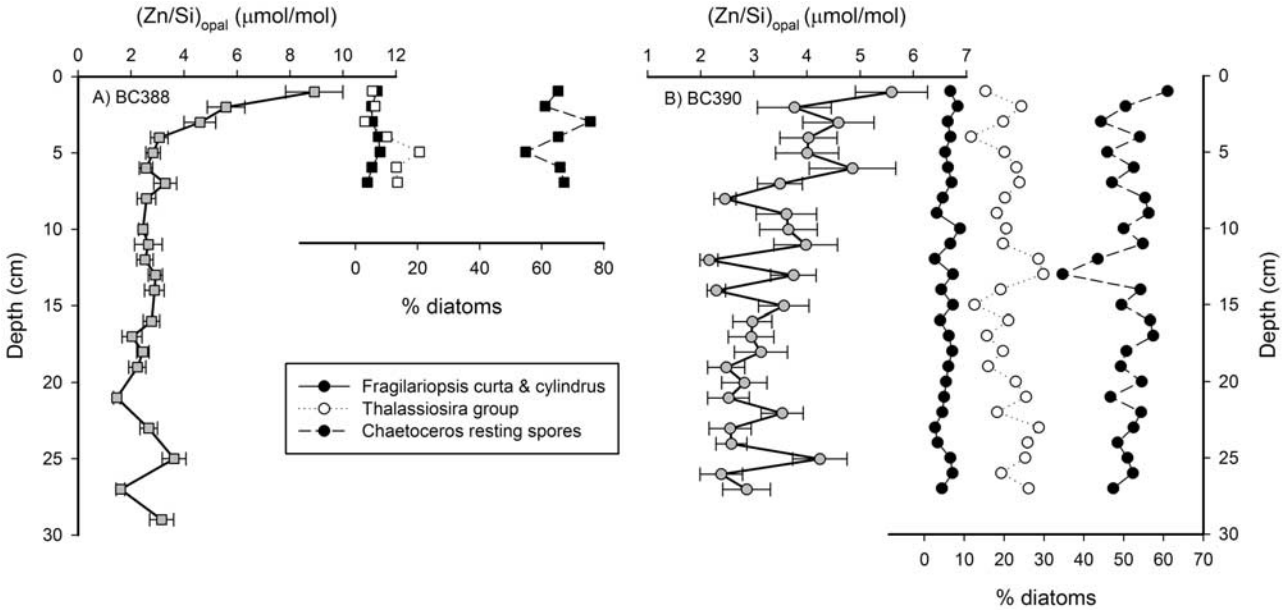

Figure 6. $(Zn/Si)_{opal}$ down-core results (error bars $\pm 2\sigma$) and species counts for (a) BC388 (squares) and (b) BC390 (circles). *Chaetoceros* resting spores and *Thalassiosira* species are the major contributors to the biogenic opal; *Fragilariopsis curta* and *F. cylindrus* are present at >3%, as expected in a seasonal sea ice environment.

[26] A Zn complexation gradient is a more likely mechanism to explain the observed onshore-offshore trend in $(Zn/Si)_{opal}$. Zn speciation in seawater is poorly constrained, but is known to exist as free ions and bound in inorganic and organic complexes [*Ellwood and van der Berg*, 2000]. Salinity, temperature, and carbonate chemistry, which vary on a seasonal timescale, are known to be important factors for inorganic Zn speciation in seawater [*Bruno*, 1990; *Stanley and Byrne*, 1990]. However, a simple speciation model (visual MINTEQ) demonstrates the effects of temperature and pH changes are minimal on zinc speciation.

[27] Rather than inorganic complexation, free zinc $[Zn^{2+}]$ is controlled to a greater extent by the abundance of organic ligands, which can bind up to 96–99% of dissolved zinc in seawater and are thought to be released by microbial degradation of organic matter [*Ellwood*, 2004; *Ellwood and van der Berg*, 2000; *Muller et al.*, 2001; *Skrabal et al.*, 2006]. Organically bound Zn is unlikely to be biologically available (M. Ellwood, personal communication, 2007), although the lability of these natural ligands remains to be tested. In the North Atlantic, lower-salinity shelf waters have a lower concentration of ligands and a higher proportion of Zn^{2+} ions than the higher-salinity open ocean [*Ellwood and van der Berg*, 2000]. In the case of Marguerite Bay, surface waters near the input of low-salinity melt may contain lower concentrations of ligands and a higher proportion of free zinc ions, which can then be incorporated into diatom cellular material. Hence we assume here the $(Zn/Si)_{opal}$ in this region is a secondary measure of salinity and that this relationship is due to the availability of organic ligands in seawater.

4.2. Down-Core History

[28] Down-core $(Al/Si)_{opal}$ and $(Zn/Si)_{opal}$ values from BC388 range from 0.007 to 0.028 g g^{-1} and 1.5 to 9.2 μmol mol mol^{-1}, respectively. Trace metal ratios in opal from BC390 are generally lower but within the same range as BC388, with $(Al/Si)_{opal}$ and $(Zn/Si)_{opal}$ values from 0.002 to 0.008 g g^{-1} and 2.2 to 5.7 μmol mol^{-1}, respectively (Figure 6 and Tables 2a and 2b). $(Zn/Si)_{opal}$ increases significantly up core for both cores, from a steady baseline of ~2–3 μmol mol^{-1} to ~8 μmol mol^{-1} at 3–4 cm and ~5 μmol mol^{-1} at 5–7 cm for BC388 and BC 390, respectively. The range of $(Zn/Si)_{opal}$ ratios are of the order of changes observed over glacial-interglacial timescales [*Ellwood and Hunter*, 2000b]. The observed increase in $(Zn/Si)_{opal}$ in younger sediments implies an increase in free $[Zn^{2+}]$ in Marguerite Bay of 1 order of magnitude [*Ellwood and Hunter*, 2000a].

[29] There is no trend in $(Al/Si)_{opal}$ through time for either core. There is only weak correlation between Al and Zn intensities for both cores (Figure 7), suggesting only a small amount of variability may be a result of clay contamination. The frequency of coarser grain layers increases toward the top of core BC388 (Figure 8).

4.3. Modeling the $(Zn/Si)_{opal}$ History

[30] The $(Zn/Si)_{opal}$ profiles require an increase in recent decades in the $(Zn/Si)_{opal}$ of biogenic opal reaching the seafloor. Using a similar advection-diffusion model as described in section 4.1, it is possible to model a "decay constant," R, for $(Zn/Si)_{opal,xs,}$ where the excess is defined as the difference between $(Zn/Si)_{opal}$ at depth z and the $(Zn/Si)_{opal}$ asymptote toward the bottom of the core. This assumes the change in Zn content of opal with time is

Table 2a. Down-Core Opal Chemistry for BC388[a]

Depth, cm	Al/Si, g g^{-1}		Zn/Si, μmol mol^{-1}	
1	0.0263	(0.0014)	8.92	(0.54)
2	0.0131	(0.0007)	5.58	(0.35)
3	0.0132	(0.0007)	4.60	(0.30)
4	0.0095	(0.0003)	3.07	(0.17)
5	0.0092	(0.0003)	2.84	(0.14)
6	0.0095	(0.0004)	2.56	(0.13)
7	0.0154	(0.0010)	3.29	(0.21)
8	0.0082	(0.0003)	2.58	(0.18)
10	0.0071	(0.0002)	2.45	(0.08)
11	0.0083	(0.0004)	2.66	(0.26)
12	0.0109	(0.0003)	2.53	(0.16)
13	0.0150	(0.0006)	2.92	(0.14)
14	0.0105	(0.0005)	2.88	(0.19)
16	0.0127	(0.0004)	2.78	(0.16)
17	0.0088	(0.0005)	2.04	(0.19)
18	0.0175	(0.0005)	2.46	(0.12)
19	0.0146	(0.0008)	2.24	(0.16)
21	0.0085	(0.0003)	1.46	(0.07)
23	0.0203	(0.0010)	2.67	(0.17)
25	0.0272	(0.0014)	3.62	(0.22)
27	0.0109	(0.0004)	1.60	(0.09)
29	0.0243	(0.0007)	3.16	(0.22)

[a]Errors are given in parentheses (1σ).

exponential. Thus for time t, the predicted $(Zn/Si)_{opal,xs}$ ratio at depth z is

$$Zn/Si_{opal,xs} = Zn/Si_{opal,0} e\left(\frac{w - \sqrt{(w^2 + 4DR)}}{2D} z\right). \quad (5)$$

[31] The values for the sedimentation rate, w, and mixing rate, D, are taken from the $^{210}Pb_{xs}$ calculation (equation (3) and Figure 9). Sensitivity tests show that a similar (Zn/Si)$_{opal,xs}$ profile can be achieved with the extreme values of w and D calculated from $^{210}Pb_{xs}$ activity (Figure 10) and can be used to estimate the error on R. This yields R values of 0.27 ± 0.05 and 0.043 ± 0.014 (μmol mol^{-1}) a^{-1} for BC388 and BC390, respectively. The value of R could reflect (1) diagenetic loss of Zn from the opal or (2) a change in the $(Zn/Si)_{opal}$ for the silica raining to the seafloor. Assuming the latter, the $(Zn/Si)_{opal}$ reaching the seafloor at time t, $(Zn/Si)_{opal,t}$, is given by

$$Zn/Si_{opal,t} = Zn/Si_{opal,0} e^{-Rt}, \quad (6)$$

where $(Zn/Si)_{opal,0}$ is the core top value. The error on the timing of the increase in $(Zn/Si)_{opal}$ reaching the seafloor can be assessed using the error of the R value. The model suggests the upturn in $(Zn/Si)_{opal,t}$ from approximately 2 to 10 μmol mol^{-1} in BC388 dates from the early to mid 1980s. The increase in BC390 from approximately 2 to 6 μmol mol^{-1} is more difficult to constrain and occurs from 1940 to

Table 2b. Down-Core Opal Chemistry for BC390[a]

Depth, cm	Al/Si, g g^{-1}		Zn/Si, μmol mol^{-1}	
1	0.0053	(0.0003)	5.59	(0.34)
2	0.0043	(0.0003)	3.76	(0.35)
3	0.0050	(0.0002)	4.59	(0.33)
4	0.0050	(0.0002)	4.03	(0.27)
5	0.0040	(0.0002)	4.01	(0.29)
6	0.0079	(0.0004)	4.86	(0.41)
7	0.0035	(0.0001)	3.49	(0.21)
8	0.0021	(0.0001)	2.46	(0.11)
9	0.0037	(0.0002)	3.62	(0.28)
10	0.0046	(0.0003)	3.65	(0.27)
11	0.0062	(0.0003)	3.98	(0.30)
12	0.0022	(0.0001)	2.15	(0.09)
13	0.0069	(0.0003)	3.74	(0.21)
14	0.0018	(0.0001)	2.30	(0.09)
15	0.0071	(0.0004)	3.57	(0.23)
16	0.0046	(0.0002)	2.97	(0.19)
17	0.0030	(0.0002)	2.95	(0.21)
18	0.0022	(0.0001)	3.14	(0.25)
19	0.0037	(0.0002)	2.48	(0.18)
20	0.0031	(0.0002)	2.82	(0.21)
21	0.0039	(0.0003)	2.52	(0.19)
22	0.0029	(0.0001)	3.54	(0.19)
23	0.0050	(0.0003)	2.55	(0.19)
24	0.0063	(0.0002)	2.58	(0.15)
25	0.0050	(0.0002)	4.24	(0.25)
26	0.0055	(0.0003)	2.39	(0.20)
27	0.0040	(0.0002)	2.86	(0.22)

[a]Errors are given in parentheses (1σ).

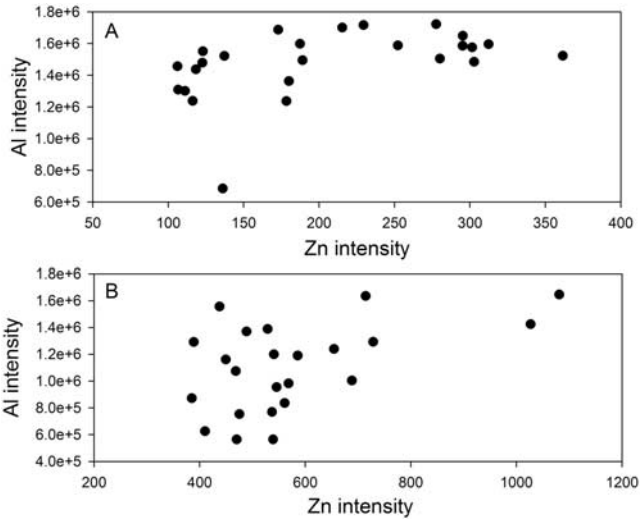

Figure 7. Plot showing lack of correlation between Al and Zn intensities down core for BC388 and BC390 (intensities as measured by quadrupole inductively coupled plasma mass spectrometer in counts per second).

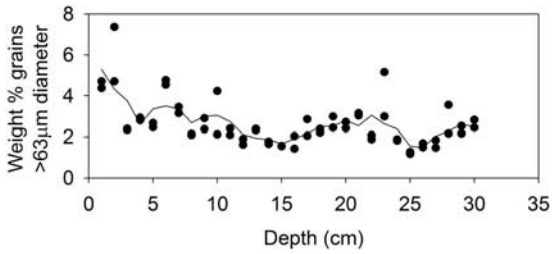

Figure 8. Grain size versus depth. Two subsamples per centimeter were sieved to determine the mass of sediment with particle size >63 μm (black circles). The black line shows the moving average. Although there are coarser layers at depth (e.g., approximately 23 cm), the frequency of coarse layers increases toward the top of the box-cores.

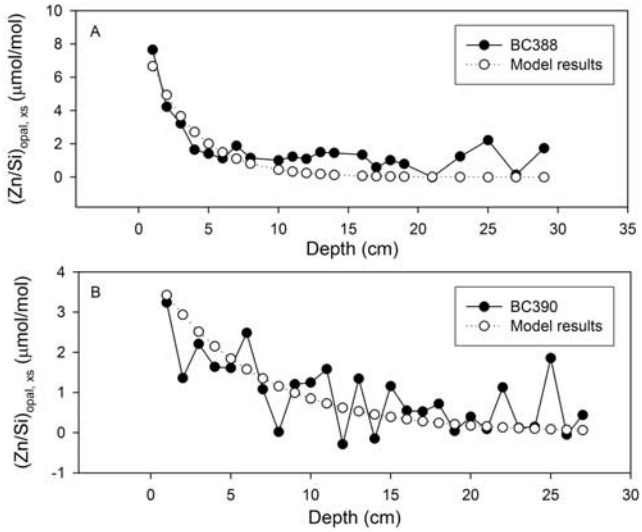

Figure 9. Comparing the measured $(Zn/Si)_{opal,xs}$ (the difference between the measured $(Zn/Si)_{opal}$ and the asymptotic value at depth) and model results for (a) BC388 (sedimentation rate, w = 0.14, and mixing rate, D = 2.57 cm a^{-1}) and (b) BC390 ($w = 0.13$ and $D = 0.97$ cm a^{-1}). The $(Zn/Si)_{opal,xs}$ profile suggests an exponential increase in the Zn content of opal reaching the seafloor in recent years.

1960 (Figure 10). Before this, the values are steady for at least 120 years and perhaps as long as 300 years.

4.4. History of Changes in the Freshwater Budget

[32] The most likely explanation for the recent upturn in $(Zn/Si)_{opal}$ is an increased freshwater influence on surface water characteristics, resulting in enhanced micronutrient availability (i.e., free Zn^{2+} ions). It is possible to argue against any postdepositional effects in controlling the recent rise in $(Zn/Si)_{opal}$. Zn mobilization in sediments is largely controlled by oxidation state and the presence of Fe and Mn oxides [*Keikens*, 1995]. Observations of the cores show that the $(Zn/Si)_{opal}$ increase starts at greater depth than the oxidized top 2–3 cm. EDX results for BC388 demonstrate no significant change in Fe or Mn down core. We have also performed incremental leaching on our diatom samples, which show that Zn is uniformly distributed in the opal, not lost preferentially during dissolution, and shows no correlation with Al (Figures 3 and 7). Our sediment trap and core top $(Zn/Si)_{opal}$ results agree well (Table 1), demonstrating that the water column signal is the same as the core top. Therefore there can be no gain of Zn into diatom opal at the water-sediment redox boundary. In contrast, the $(Al/Si)_{opal}$ results show a marked increase from sediment trap to core top consistent with diagenetic alteration [e.g., *Van Beueskom et al.*, 1997].

[33] Our $(Zn/Si)_{opal}$ proxy for salinity indicates a trend of increased meltwater flux through time. However, artifacts may arise in the $(Zn/Si)_{opal}$ record as a result of changes in (1) diatom population structure or (2) anthropogenic heavy metal pollution. First, there is no species bias as $(Zn/Si)_{opal}$ does not show a relationship with any of the more abundant diatoms, e.g., *Thalassiosira* or *Chaetoceros* resting spores, which form the bulk of the biogenic silica (Figures 2 and 6). Although there are significant relationships between the $(Zn/Si)_{opal}$ and the sea ice diatoms *Actinocyclus actinochilus*, this species composes only a small percentage (<1%) of the whole assemblage and is unlikely to affect bulk $(Zn/Si)_{opal}$ [*Ellwood and Hunter*, 2000b].

[34] Second, an increase in Zn input could be explained by increased erosion and anthropogenic pollutants from nearby Rothera Point, as has been observed for other Antarctic research stations [*Sheppard et al.*, 1997]. However, pollution is unlikely to be a significant factor as the research station was constructed in the 1970s before the sharp increase in $(Zn/Si)_{opal}$, and our seawater analyses show no sign of contamination from the station wharf. The increase could also be a result of increased anthropogenic pollutants and dust input from the north [*McConnell et al.*, 2007]. However, this would not explain the onshore-offshore trend in $(Zn/Si)_{opal}$ observed in the core top calibration, as all regions around Adelaide Island would be equally affected. Furthermore, snow and ice records demonstrate recent snowpack contains similar Zn content to Holocene ice and has not been contaminated by recent anthropogenic inputs [*Boutron et al.*, 1990].

[35] A recent increase in continental freshwater input and Zn uptake into opal is consistent with the onshore-offshore gradient of $(Zn/Si)_{opal}$ in the core tops, as well as with the significant increase in sediment coarse fraction (Figure 8) and the similarity to Southern Hemisphere temperature anomalies [*National Environmental Satellite, Data, and Information Service*, 2006]. Our XRD results indicate there is no concurrent change in mineral composition of the sediments down core, suggesting no significant change in chemical weathering processes or sediment source.

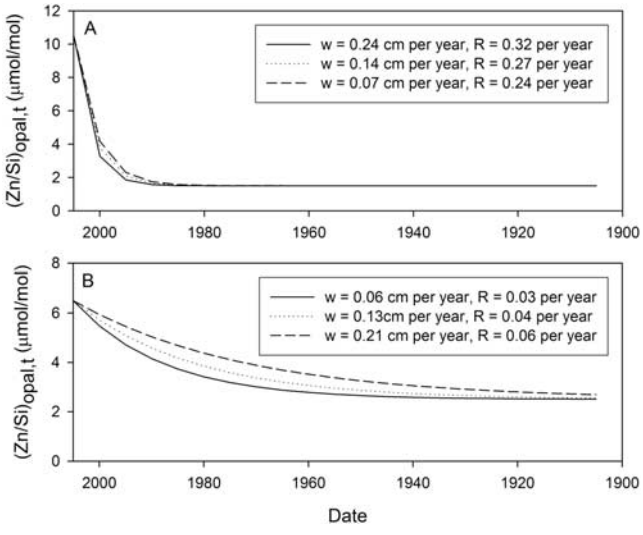

Figure 10. Sensitivity tests on $(Zn/Si)_{opal}$ model for (a) BC388 and (b) BC390. The Zn content of the opal reaching the seafloor, $(Zn/Si)_{opal,t}$, is calculated using the range of $(Zn/Si)_{opal}$ decay rate (R) values from the ^{210}Pb advection-diffusion model (equations (5) and (6)). Here w is the sedimentation rate in centimeters per year.

[36] Assuming our $(Zn/Si)_{opal}$ increase is a result of freshwater input (Figure 5), this corresponds to a decrease in salinity at BC388 and BC390 by 0.7 and 0.4 psu, respectively. We have constructed a simple mass balance model to constrain the volume of additional meltwater to Ryder Bay above BC388 (Figure 11). We have assumed that $(Zn/Si)_{opal}$ is related to salinity according to our core top calibration. The model is consistent with a doubling of the freshwater contribution to the summer mixed layer since the early 1980s. Our data show that recent enhanced meltwater flux, probably from the Sheldon Glacier (Figure 1), is not a result of post-LIA warming but is more likely a response to late 20th century warming. The timing of this increase is consistent with observations from the nearby Wordie Ice Shelf, which has been retreating since the 1960s and experienced a major breakout between 1988 and 1989 [*Vaughan and Doake*, 1996]. Despite different degrees of basal friction and melting between tidewater glaciers and ice shelves, there may be a common factor influencing ice retreat in the Marguerite Bay region. Glacier acceleration has been documented as a result of the collapse of the ice shelves into which they feed [*Rignot et al.*, 2005; *Scambos et al.*, 2004], but the Sheldon Glacier feeds directly into Marguerite Bay, which has experienced full glaciomarine conditions for approximately 6000 years [*Bentley et al.*, 2005]. Instead, atmospheric warming may have caused net ablation for both ice shelves and glaciers in this region, providing a link between air temperatures and ocean nutrient supply. Both atmospheric and oceanic warming, for example, warming of UCDW in the case of WAP glaciers with floating termini, may be causing unprecedented changes in coastal freshwater and nutrient budgets. Our new approach can be utilized to investigate such changes in other high-latitude regions.

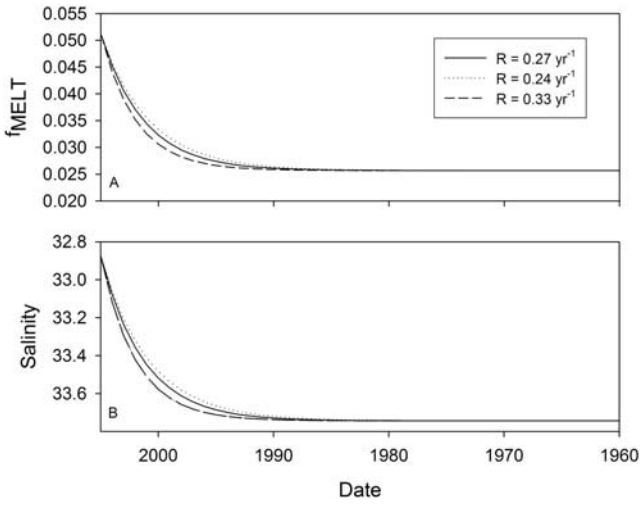

Figure 11. Model results showing (a) changes in the contribution of freshwater in Ryder Bay and (b) changes in salinity as a result of freshwater inputs since 1960. Mass balance models of meltwater flux into the mixed layer of Ryder Bay, an inland bay near Rothera Research Station, by the retreating Sheldon Glacier, using the linear relationship between $(Zn/Si)_{opal}$ and salinity in Marguerite Bay. Theoretical values for $(Zn/Si)_{opal}$ for each year were calculated using the relationship described in section 4.1, assuming an exponential "decay" in $(Zn/Si)_{opal}$ given by R (equation (5)). Salinity was calculated using the correlation between our core top data and published salinity values, $S = -0.0828\ (Zn/Si)_{opal} + 33.744$ (Figure 5). A mass balance equation was solved for the fraction of freshwater input into Ryder Bay, f_{FRESH} (equation (4)). Here f_{FRESH} was corrected for contribution from precipitation and converted to fraction of meltwater, and f_{MELT} was corrected for a summer mixed layer depth of 60 m [*Meredith et al.*, 2008].

[37] Coastal regions are the most productive of the Southern Ocean, with primary productivity and carbon export fluxes at least 1 order of magnitude greater than the permanently open ocean [*Smith and Nelson*, 1986; *Tréguer and Jacques*, 1992]. The link between glaciers and coastal productivity has been shown in other regions of the Antarctic and Arctic [*Dierssen et al.*, 2002; *Garibotti et al.*, 2003; *Jankowska et al.*, 2005]. Glaciers and icebergs can act as a source of macronutrients to seawater [*Smith et al.*, 2007b], and we argue here that they impact the complexation and bioavailability of trace metals. Meltwater also stabilizes the water column, providing favorable light and nutrient conditions for phytoplankton and allowing large diatom cells to accumulate before sinking rapidly, efficiently transporting organic carbon to the seafloor [*Kemp et al.*, 2006]. In addition to shifting plankton population structure as a result of changes in ocean physicochemical properties [*Smith et al.*, 2003], enhanced meltwater flux could drive an increase in coastal primary and export production.

5. Conclusion and Summary

[38] Diatom opal may have useful applications as paleoproxies in regions where biogenic carbonates are not preserved in marine sediments, such as the Southern Ocean, and here we demonstrate that $(Zn/Si)_{opal}$ can be used as a proxy for freshwater input. Opal can be separated from sediments using heavy liquid flotation and chemically cleaned through a series of reductive and oxidative steps for trace metal analysis. The following arguments demonstrate the method is reliable: (1) SEM images show the opal to be clean of clay particles, (2) sequential dissolution experiments show $(Al/Si)_{opal}$ and $(Zn/Si)_{opal}$ ratios plateau to a constant value, (3) poor correlation between Al and Zn intensities suggest the Zn is not sourced from clays or surface adsorption, (4) yield experiments demonstrate no Si is lost through the addition of dilute HF, and (5) repeat measurements show a high level of machine and sample reproducibility.

[39] A box-core top calibration from the coastal region of the West Antarctic Peninsula demonstrates a good relationship between $(Zn/Si)_{opal}$ and salinity and/or chlorophyll *a*. Two down-core records show changes in the $(Zn/Si)_{opal}$ through time, which we interpret here as showing a change in Zn complexation because of an increase in the freshwater input to the coastal waters in recent decades. The implication is that atmospheric and oceanic warming may be

causing unprecedented changes in coastal freshwater and nutrient budgets. If, as we suspect is the case, the melting of glaciers and calved icebergs affects the bioavailability of trace metals such as Zn, an increase in meltwater flux may have a significant impact on coastal productivity.

[40] **Acknowledgments.** The authors would like to thank the following: John Arden and Dave Harding for assistance with Q-ICP-MS (Department of Earth Sciences, University of Oxford); other members of the AFI4–02 project, Raja Ganeshram and Damien Carson (University of Edinburgh) and Henry Elderfield (University of Cambridge); Andrew Cundy (University of Sussex, now University of Brighton) for ^{210}Pb analysis; Frank Cullen (Department of Materials Science, University of Oxford) for EDX and XRD analysis; Andrew Clarke and Mike Meredith (British Antarctic Survey) for biological and physical oceanographic data; and the base commander and staff of Rothera Research Station and master and crew of the RRS *James Clark Ross*, British Antarctic Survey. The authors would also like to thank M. Ellwood, G. Dickens, X. Crosta, and an anonymous reviewer for insightful commentary. The work was funded as part of NERC Antarctic Funding Initiative AFI4–02. K.R.H. is funded by NERC grant NER/S/A/2004/12390.

References

Anderson, J. B. (1999), *Antarctic Marine Geology*, 289 p., Cambridge Univ. Press, Cambridge, U. K.

Anderson, R. F., R. F. Bopp, K. O. Buesseler, and P. E. Biscaye (1988), Mixing of particles and organic constituents in sediments from the continental shelf and slope off Cape Cod: SEEP-1 results, *Cont. Shelf Res.*, *8*, 925–946, doi:10.1016/0278-4343(88)90082-9.

Bentley, M. J., D. A. Hodgson, D. E. Sugden, S. J. Roberts, J. A. Smith, M. J. Leng, and C. Bryant (2005), Early Holocene retreat of the George VI Ice Shelf, Antarctic Peninsula, *Geology*, *33*, 173–176, doi:10.1130/G21203.1.

Boutron, C. F., C. C. Patterson, and N. I. Barkov (1990), The occurance of zinc in Antarctic ice and recent snow, *Earth Planet. Sci. Lett.*, *101*, 248–259, doi:10.1016/0012-821X(90)90157-S.

Bruno, J. (1990), The influence of dissolved carbon dioxide on trace metal speciation in seawater, *Mar. Chem.*, *30*, 231–240, doi:10.1016/0304-4203(90)90072-K.

Brzezinski, M. A., C. J. Pride, V. M. Franck, D. M. Sigman, J. L. Sarmiento, K. Matsumoto, N. Gruber, G. H. Rau, and K. H. Coale (2002), A switch from $Si(OH)_4$ to NO_3^- depletion in the glacial Southern Ocean, *Geophys. Res. Lett.*, *29*(12), 1564, doi:10.1029/2001GL014349.

Buffoni, G., R. Delfanti, and C. Papucci (1992), Accumulation rates and mixing processes in near-surface North Atlantic sediments: Evidence from C-14 and Pu-289, 240 downcore profiles, *Mar. Geol.*, *109*, 159–170, doi:10.1016/0025-3227(92)90226-8.

Burckle, L. H., and J. Cirilli (1987), Origin of diatom ooze belt in the Southern Ocean: Implications for late Quaternary paleoceanography, *Micropaleontology*, *33*, 82–86, doi:10.2307/1485529.

Burckle, L. H. D., D. Robinson, and D. Cooke (1982), Reappraisal of sea-ice distribution in Atlantic and Pacific sectors of the Southern Ocean at 18,000 yr BP, *Nature*, *299*, 435–437, doi:379328a0/299435a0.

Clapperton, C. M., and D. E. Sugden (1982), Late Quaternary glacial history of George VI Sound Area, West Antarctica, *Quat. Res.*, *18*, 243–267, doi:10.1016/0033-5894(82)90074-6.

Clarke, A., E. J. Murphy, M. P. Meredith, J. C. King, L. S. Peck, D. K. A. Barnes, and R. C. Smith (2007), Climate change and the marine ecosystem of the Western Antarctic Peninsula, *Proc. R. Soc., Ser. B*, *362*, 149–166, doi:10.1098/rstb.2006.1958.

Collier, R., and J. Edmond (1984), The trace element geochemistry of marine biogenic particulate matter, *Prog. Oceanogr.*, *13*, 113–199, doi:10.1016/0079-6611(84)90008-9.

Cook, A., A. J. Fox, D. G. Vaughan, and J. G. Ferrigno (2005), Retreating glacier fronts on the Antarctic Peninsula over the past half-century, *Science*, *308*, 541–544, doi:10.1126/science.1104235.

Crosta, X., and A. Shemesh (2002), Reconciling down core anticorrelation of diatom carbon and nitrogen isotopic ratios from the Southern Ocean, *Paleoceanography*, *17*(1), 1010, doi:10.1029/2000PA000565.

Crosta, X., A. Shemesh, M.-E. Salvignac, H. Gildor, and R. Yam (2002), Late Quaternary variations of elemental ratios (C/Si and N/Si) in diatom-bound organic matter from the Southern Ocean, *Deep Sea Res., Part II*, *49*, 1939–1952, doi:10.1016/S0967-0645(02)00019-X.

Dehairs, F., R. Chesselet, and J. Jedwab (1980), Discrete suspended particles of barite and the barium cycle in the open ocean, *Earth Planet. Sci. Lett.*, *49*, 528–550, doi:10.1016/0012-821X(80)90094-1.

de la Rocha, C., M. A. Brzezinski, and M. J. DeNiro (1996), Purification, recovery, and laser-driven fluorination of silicon from dissolved and particulate silica for the measurement of natural stable isotope abundances, *Anal. Chem.*, *68*, 3746–3750, doi:10.1021/ac960326j.

Dierssen, H. M., R. C. Smith, and M. Vernet (2002), Glacial meltwater dynamics in coastal waters west of the Antarctic Peninsula, *Proc. Natl. Acad. Sci. U. S. A.*, *99*, 1790–1795, doi:10.1073/pnas.032206999.

Dixit, S., and P. Van Cappellen (2002), Surface chemistry and reactivity of biogenic silica, *Geochim. Cosmochim. Acta*, *66*, 2559–2568, doi:10.1016/S0016-7037(02)00854-2.

Dixit, S., P. Van Cappellen, and A. J. van Bennekom (2001), Processes controlling solubility of biogenic silica and pore water build-up of silicic acid in marine sediments, *Mar. Chem.*, *73*, 333–352, doi:10.1016/S0304-4203(00)00118-3.

Dolezal, J., et al. (1968), *Decomposition Techniques in Inorganic Analysis*, Elsevier, New York.

Domack, E. W., et al. (1992), Intrusion of circumpolar deep water along the Bellingshausen Sea continental shelf, *Antarct. J. U. S.*, *27*, 71.

Domack, E. W., S. E. Ishman, A. B. Stein, C. E. McClennen, and A. J. T. Jull (1995), Late Holocene advance of the Muller Ice Shelf, Antarctic Peninsula: Sedimentological, geochemical and palaeontological evidence, *Antarct. Sci.*, *7*, 159–170, doi:10.1017/S0954102095000228.

Ellwood, M. (2004), Zinc and cadmium speciation in subantarctic waters east of New Zealand, *Mar. Chem.*, *87*, 37–58, doi:10.1016/j.marchem.2004.01.005.

Ellwood, M. J., and K. A. Hunter (1999), Determination of the Zn/Si ratio in diatom opal: A method for the separation, cleaning and dissolution of diatoms, *Mar. Chem.*, *66*, 149–160, doi:10.1016/S0304-4203(99)00037-7.

Ellwood, M. J., and K. A. Hunter (2000a), The incorporation of zinc and iron into the frustule of the marine diatom *Thalassiosira pseudonana*, *Limnol. Oceanogr.*, *45*, 1517–1524.

Ellwood, M. J., and K. A. Hunter (2000b), Variations in the Zn/Si record over the last interglacial glacial transition, *Paleoceanography*, *15*, 506–514, doi:10.1029/1999PA000470.

Ellwood, M. J., and C. M. G. van der Berg (2000), Zinc speciation in the northeastern Atlantic Ocean, *Mar. Chem.*, *68*, 295–306, doi:10.1016/S0304-4203(99)00085-7.

Froelich, P. N., V. Blanc, R. A. Mortlock, S. N. Chillrud, W. Dunstan, A. Udomkit, and T.-H. Peng (1992), River fluxes of dissolved silica to the ocean were higher during glacials: Ge/Si in diatoms, rivers and oceans, *Paleoceanography*, *7*, 739–767, doi:10.1029/92PA02090.

Garibotti, I. A., M. Vernet, M. E. Ferrario, R. C. Smith, R. M. Ross, and L. B. Quetin (2003), Phytoplankton spatial distribution patterns along the western Antarctic Peninsula (Southern Ocean), *Mar. Ecol. Prog. Ser.*, *261*, 21–39, doi:10.3354/meps261021.

Gonneea, M. E., and A. Paytan (2006), Phase associations of barium in marine sediments, *Mar. Chem.*, *100*, 124–135, doi:10.1016/j.marchem.2005.12.003.

Harding, D. J., J. W. Arden, and R. E. M. Rickaby (2006), A method for precise analysis of trace element/calcium ratios in carbonate samples using quadrupole inductively coupled plasma mass spectrometry, *Geochem. Geophys. Geosyst.*, *7*, Q06003, doi:10.1029/2005GC001093.

Henderson, G. M., F. N. Lindsay, and N. C. Slowey (1999), Variation in bioturbation with water depth on marine slopes: A study on the Little Bahamas Bank, *Mar. Geol.*, *160*, 105–118, doi:10.1016/S0025-3227(99)00018-3.

Ho, T.-Y., A. Quigg, Z. V. Finkel, A. J. Milligan, K. Wyman, P. G. Falkowski, and F. M. M. Morel (2003), The elemental composition of some marine phytoplankton, *J. Phycol.*, *39*, 1145–1159, doi:10.1111/j.0022-3646.2003.03-090.x.

Jankowska, K., et al. (2005), Abundance and biomass of bacteria in two Arctic glacial fjords, *Pol. Polar Res.*, *26*, 77–84.

Keikens, L. (1995), Zinc, in *Heavy Metals in Soils*, 2nd ed., edited by B. J. Alloway, pp. 288–297, Blackie Acad. and Prof., New York.

Kemp, A. E. S., R. B. Pearce, I. Grigorov, J. Rance, C. B. Lange, P. Quilty, and I. Salter (2006), Production of giant marine diatoms and their export at oceanic frontal zones: Implications for Si and C flux from stratified oceans, *Global Biogeochem. Cycles*, *20*, GB4S04, doi:10.1029/2006GB002698.

Kim, D. H., and W. C. Burnett (1988), Accumulation and biological mixing of Peru margin sediments, *Mar. Geol.*, *80*, 181–194, doi:10.1016/0025-3227(88)90089-8.

Lal, D., C. Charles, L. Vacher, J. N. Goswami, A. J. T. Jull, L. McHargue, and R. C. Finkel (2006), Paleo-ocean chemistry records in marine opal: Implications for fluxes of trace elements, cosmogenic nuclides (^{10}Be and ^{26}Al), and biological productivity, *Geochim. Cosmochim. Acta*, *70*, 3275–3289, doi:10.1016/j.gca.2006.04.004.

Löscher, B. M. (1999), Relationships among Ni, Cu, Zn and major nutrients in the Southern Ocean, *Mar. Chem.*, *67*, 67–102, doi:10.1016/S0304-4203(99)00050-X.

Martin, J. H., and G. A. Knauer (1973), The elemental composition of plankton, *Geochim. Cosmochim. Acta*, *37*, 1639–1653, doi:10.1016/0016-7037(73)90154-3.

McConnell, J. R., A. J. Aristarain, J. R. Banta, P. R. Edwards, and J. C. Simões (2007), 20th-century doubling in dust archived in an Antarctic Peninsula ice core parallels climate change and desertification in South America, *Proc. Natl. Acad. Sci. U. S. A.*, *104*, 5743–5748, doi:10.1073/pnas.0607657104.

Meredith, M. P., and J. C. King (2005), Rapid climate change in the ocean west of the Antarctic Peninsula during the second half of the 20th century, *Geophys. Res. Lett.*, *32*, L19604, doi:10.1029/2005GL024042.

Meredith, M. P., M. A. Brandon, M. I. Wallace, A. Clarke, M. J. Leng, I. A. Renfrew, N. P. M. van Lipzig, and J. C. King (2008), Variability in the freshwater balance of northern Marguerite Bay, Antarctic Peninsula: Results from δ^{18}O, *Deep Sea Res., Part II*, *55*, 309–322.

Mitchell, A., G. H. Brown, and R. Fuge (2001), Minor and trace element export from a glaciated Alpine headwater catchment (Haut Glacier d'Arolla, Switzerland), *Hydrol. Processes*, *15*, 3499–3524, doi:10.1002/hyp.1041.

Morel, F. M. M., and N. M. Price (2003), The biogeochemical cycles of trace metals in the oceans, *Science*, *300*, 944–947, doi:10.1126/science.1083545.

Morely, D. W., M. J. Leng, A. W. Mackay, H. J. Sloane, P. Roual, and R. W. Battarbee (2004), Cleaning of lake sediment samples for diatom oxygen isotope analysis, *J. Paleolimnology*, *31*, 391–401.

Muller, F. L. L., S. B. Gulin, and Å. Kalvøy (2001), Chemical speciation of copper and zinc in surface waters of the western Black Sea, *Mar. Chem.*, *76*, 233–251, doi:10.1016/S0304-4203(01)00060-3.

National Environmental Satellite, Data, and Information Service (2006), Global surface temperature anomalies, http://www.ncdc.noaa.gov/oa/climate/research/anomalies/anomalies.html, Natl. Clim. Data Cent., Asheville, N. C.

Nozaki, Y., J. K. Cochran, K. K. Turekian, and G. Keller (1977), Radiocarbon and ^{210}Pb distribution in submersible taken deep-sea cores from Project Famous, *Earth Planet. Sci. Lett.*, *34*, 167–173, doi:10.1016/0012-821X(77)90001-2.

Peng, T.-H., W. S. Broecker, and W. H. Berger (1979), Rate of benthic mixing in deep-sea sediment as determined by radioactive tracers, *Quat. Res.*, *11*, 141–149, doi:10.1016/0033-5894(79)90074-7.

Pritchard, H. D., and D. G. Vaughan (2007), Widespread acceleration of tidewater glaciers on the Antarctic Peninsula, *J. Geophys. Res.*, *112*, F03S29, doi:10.1029/2006JF000597.

Pudsey, C. J., and J. Evans (2001), First survey of Antarctic sub-ice shelf sediments reveals mid-Holocene ice shelf retreat, *Geology*, *29*, 787–790, doi:10.1130/0091-7613(2001)029<0787:FSOASI>2.0.CO;2.

Rignot, E., G. Casassa, S. Gogineni, P. Kanagaratnam, W. Krabill, H. Pritchard, A. Rivera, R. Thomas, J. Turner, and D. Vaughan (2005), Recent ice loss from the Fleming and other glaciers, Wordie Bay,West Antarctic Peninsula, *Geophys. Res. Lett.*, *32*, L07502, doi:10.1029/2004GL021947.

Robertson, R., M. Visbeck, A. L. Gordon, and E. Fahrbach (2002), Long-term temperature trends in the deep waters of the Weddell Sea, *Deep Sea Res., Part II*, *49*, 4791–4806, doi:10.1016/S0967-0645(02)00159-5.

Scambos, T. A., J. A. Bohlander, C. A. Shuman, and P. Skvarca (2004), Glacier acceleration and thinning after ice shelf collapse in the Larsen B embayment, Antarctica, *Geophys. Res. Lett.*, *31*, L18402, doi:10.1029/2004GL020670.

Shemesh, A., R. A. Mortlock, R. J. Smith, and P. N. Froelich (1988), Determination of Ge/Si in marine siliceous microfossils: Separation, cleaning and dissolution of diatoms and radiolaria, *Mar. Chem.*, *25*, 305–323, doi:10.1016/0304-4203(88)90113-2.

Sheppard, D. S., J. M. Deely, and W. H. L. Edgerley (1997), Heavy metal content of meltwaters from the Ross Dependency,Antarctica, *N. Z. J. Mar. Freshwater Res.*, *31*, 313–325.

Skrabal, S. A., K. L. Lieseke, and R. J. Kieber (2006), Dissolved zinc and zinc-complexing ligands in an organic-rich estuary: Benthic fluxes and comparison with copper speciation, *Mar. Chem.*, *100*, 108–123, doi:10.1016/j.marchem.2005.12.004.

Smedsrud, L. H. (2005), Warming of the deep water in the Weddell Sea along the Greenwich meridian: 1977–2001, *Deep Sea Res., Part I*, *52*, 241–258, doi:10.1016/j.dsr.2004.10.004.

Smith, D. A., E. E. Hofmann, J. M. Klinck, and C. M. Lascara (1999), Hydrography and circulation of the West Antarctic Peninsula continental shelf, *Deep Sea Res., Part I*, *46*, 925–949, doi:10.1016/S0967-0637(98)00103-4.

Smith, J. A., M. J. Bentley, D. A. Hodgson, and A. J. Cook (2007a), George VI Ice Shelf: Past history, present behaviour and potential mechanisms for future collapse, *Antarct. Sci.*, *19*, 131–142, doi:10.1017/S0954102007000193.

Smith, K. L., Jr., B. H. Robison, J. J. Helly, R. S. Kaufmann, H. A. Ruhl, T. J. Shaw, B. S. Twining, and M. Vernet (2007b), Free-drifting icebergs: Hot spots of chemical and biological enrichment in the Weddell Sea, *Science*, *317*, 478–482, doi:10.1126/science.1142834.

Smith, R. C., et al. (2003), Palmer long-term ecological research on the Antarctic marine ecosystem, *Antarct. Res. Ser.*, *79*, 1–14.

Smith, W. O., and D. M. Nelson (1986), Importance of ice edge phytoplankton production in the Southern Ocean, *BioScience*, *36*, 251–257, doi:10.2307/1310215.

Stanley, J. K., and R. H. Byrne (1990), Inorganic complexation of zinc (II) in seawater, *Geochim. Cosmochim. Acta*, *54*, 753–760, doi:10.1016/0016-7037(90)90370-Z.

Tréguer, P., and G. Jacques (1992), Dynamics of nutrients and phytoplankton and fluxes of carbon, nitrogen and silicon in the Antarctic Ocean, *Polar Biol.*, *12*, 149–162, doi:10.1007/BF00238255.

Van Bennekom, A. J. (1981), On the role of aluminium in the dissolution kinetics of diatom frustules, in *Proceedings of the Sixth Diatom Symposium 1980*, edited by R. Ross, pp. 445–454, Koeltz Sci., Köenigstein, Germany.

Van Bennekom, A. J., J. H. F. Jansen, S. J. van der Gaast, J. M. van Iperen, and J. Pieters (1989), Aluminium-rich opal: An intermediate in the preservation of biogenic silica in the Zaire (Congo) deep sea fan, *Deep Sea Res., Part A*, *36*, 173–190, doi:10.1016/0198-0149(89)90132-5.

van Beueskom, J. E. E., A. J. Van Bennekom, P. Tréguer, and J. Morvan (1997), Aluminium and silicic acid in water and sediments of the Enderby and Crozet Basins, *Deep Sea Res., Part II*, *44*, 987–1003, doi:10.1016/S0967-0645(96)00105-1.

Vaughan, D. G., and C. S. M. Doake (1996), Recent atmospheric warming and retreat of ice shelves on the Antarctic Peninsula, *Nature*, *379, 328–331,* doi:10.1038/379328a0.

K. R. Hendry and R. E. M. Rickaby, Department of Earth Sciences, University of Oxford, Parks Road, Oxford OX1 3PR, UK. (kathh@earth.ox.ac.uk)